Journal of Biomolecular NMR **27:** 205–219, 2003.

Solution structure of the human Grb7-SH2 domain/erbB2 peptide complex and structural basis for Grb7 binding to ErbB2

Monika Ivancic[a], Roger J. Daly[b] & Barbara A. Lyons*[,a]
[a]*Department of Biochemistry, University of Vermont College of Medicine Burlington, VT 05405, U.S.A.;* [b]*Cancer Research Program, Garvan Institute of Medical Research, St. Vincent's Hospital, Sidney, NSW 2010, Australia*

Received 14 January 2003; Accepted 13 May 2003

Key words: breast cancer, growth factor receptor bound, NMR, receptor tyrosine kinase, Src Homology

Abstract

The solution structure of the hGrb7-SH2 domain in complex with a ten amino acid phosphorylated peptide ligand representative of the erbB2 receptor tyrosine kinase (pY1139) is presented as determined by nuclear magnetic resonance methods. The hGrb7-SH2 domain structure reveals the Src homology 2 domain topology consisting of a central β-sheet capped at each end by an α-helix. The presence of a four residue insertion in the region between β-strand E and the EF loop and resulting influences on the SH2 domain/peptide complex structure are discussed. The binding conformation of the erbB2 peptide is in a β-turn similar to that found in phosphorylated tyrosine peptides bound to the Grb2-SH2 domain. To our knowledge this is only the second example of an SH2 domain binding its naturally occurring ligands in a turn, instead of extended, conformation. Close contacts between residues responsible for binding specificity in hGrb7-SH2 and the erbB2 peptide are characterized and the potential effect of mutation of these residues on the hGrb7-SH2 domain structure is discussed.

Abbreviations: erbB2 – epidermal growth factor receptor 2; erbB3 – epidermal growth factor receptor 3; GST – glutathione S-transferase; Grb – growth factor receptor bound; HSQC – heteronuclear single-quantum coherence; IGF1 – insulin-like growth factor 1; Kit – receptor tyrosine kinase gene product of the kit gene; MEK1 – MAPK/ERK kinase 1; Nedd4 – Neuronal precursor cell-expressed developmentally down-regulated 4; NMR – nuclear magnetic resonance; NOE – nuclear Overhauser effect; NOESY – NOE spectroscopy; pY1139 – ten amino acid erbB2 representative phosphorylated peptide PQPEpYVNQPD; Raf1 – Ras altered form kinase 1; Ret – uretic bud development bud receptor; RMSD – root-mean-square deviation; RTK – receptor tyrosine kinase; SH2 – Src homology 2; vSrc-SH2 – rous sarcoma virus SH2; TSP – 3-(trimethylsilyl)propionic acid.

Introduction

Receptor tyrosine kinases (RTKs) play a major role in intracellular communication and cell signaling. The general mechanism of action involves binding of a ligand to the RTK, RTK dimerization and autophosphorylation and initiation of a signaling cascade within the cell. The growth factor receptor bound (Grb) family of proteins binds to the epidermal growth factor receptor (EGFR, erbB1) via their SH2 domains. A subclass of Grb proteins has been identified based on similar domain architecture (Margolis, 1994). The members of the Grb7 family of proteins, Grb7, Grb10 and Grb14, have an N-terminal Proline rich domain, followed by a Ras Associating-like (RA) domain identified via sequence homology searches (Wojcik et al., 1999), followed by the Pleckstrin Homology (PH) domain, a short phosphotyrosine interaction region (PIR, BPS) and a C-terminal Src Homology 2 (SH2) domain. The members of the Grb7 family may carry out a more specialized signaling pathway than other more ubiquitously expressed SH2 domain-containing proteins as their expression is considerably more tissue-specific. Grb7 is expressed in the liver, kidney, and

*To whom correspondence should be addressed. E-mail: Barbara.Lyons@uvm.edu

gonads (Margolis et al., 1992), while Grb14 is expressed in the liver, kidney, pancreas, gonads, heart and skeletal muscle (Daly et al., 1996). In many of the tissues for which they are specific, correlations have been made between over-expression and cancer. Grb7 has been shown to be co-over-expressed with erbB2 in 20–30% of all breast cancers (Stein et al., 1994), and Grb14 has been demonstrated to be over-expressed in some prostate cancer cell lines (Daly et al., 1996).

The SH2 domains of Grb7, Grb10 and Grb14 share 68–72% residue identity and they each preferentially bind to a different RTK. Grb7 binds strongly to the erbB2 receptor via its SH2 domain in co-immunoprecipitation experiments (Stein et al., 1994), while Grb10 and 14 only weakly associate with erbB2 (Janes et al., 1997). The hGrb7-SH2 domain binds to the phosphorylated tyrosine 1139 on the erbB2 receptor and prefers an asparagine in the +2 position, while Grb14-SH2 domain binds to the phosphorylated tyrosine 766 on the Fibroblast Growth Factor Receptor (FGFR) and prefers a hydrophobic residue in the +3 position (Janes et al., 1997; Reilly et al., 2000). Throughout the manuscript, peptide residue positions subsequent (C-terminal) to the phosphotyrosine residue are referred to as +1 (the first residue after the pTyr), +2 (the second residue after the pTyr), etc. Residue positions prior (N-terminal) to the phosphotyrosine are referred to as −1 (the residue immediately preceding the pTyr), and so forth.

The SH2 domain of Grb10 has been shown to interact with many different proteins, including the insulin and IGF1 receptors (He et al., 1998), platelet-derived growth factor (PDGF) receptor-β (Wang et al., 1999), Ret (Pandey et al., 1995), Kit (Thommes et al., 1999), Raf1 and MEK1 (Nantel et al., 1998), and Nedd4 (Morrione et al., 1999). Despite this abundance of binding partners and a recently solved crystal structure (Stein et al., 2003), a consensus binding sequence for Grb10 has not been determined.

Prior research has shown that two residues within the βD strand of the Grb7 and Grb14 SH2 domains are critical for specific binding to the erbB2 receptor (Janes et al., 1997). The residues are βD5 = Tyr, βD6 = Leu for the Grb7 SH2 domain and βD5 = Phe, βD6 = Gln for the Grb14 SH2 domain. It was shown that mutation of these residues in Grb7 to the corresponding Grb14 SH2 domain residues abrogates binding to the erbB2 receptor phosphopeptides, while mutation of the Grb14 βD5/βD6 residues to the corresponding residues in Grb7 results in binding to the erbB2 receptor phosphopeptide. Mutation of just one residue results in intermediate affinity, although βD6 appears to be more important than βD5 (Janes et al., 1997).

SH2 domains bind their phosphorylated tyrosine ligands in an extended conformation with the exception of the Grb2-SH2 domain, which binds its ligands in a β-turn conformation (Ogura et al., 1999; Rahuel et al., 1998). The reason for the β-turn binding conformation of Grb2-SH2 domain ligands is the presence of a bulky tryptophan residue (Trp 66) within the loop region between β-strand E and β-strand F. This tryptophan residue occludes the hydrophobic pocket normally occupied in the phosphorylated peptide complexed state by a hydrophobic residue in the +3 position subsequent to the phosphorylated tyrosine. The preferred consensus binding site of the Grb2-SH2 domain contains an asparagine in the +2 position relative to the phosphorylated tyrosine. The asparagine in the +2 position has been postulated to provide binding site recognition for this domain through favorable enthalpic interactions with a β-strand lysine sidechain (McNemar et al., 1997). Because hGrb7-SH2 domain also prefers an asparagine residue in the +2 position, it has been suggested that hGrb7-SH2 binds its phosphorylated tyrosine ligands in a β-turn conformation (Janes et al., 1997). In this case, it is proposed that the four residue insertion in the corresponding βE strand and EF loop region in hGrb7-SH2 provides the steric 'bulkiness' necessary for the β-turn binding configuration of the phosphopeptide.

Even though high sequence homology exists between the members of the Grb7 family, each member displays its own preference in binding. Why this is so can only be revealed with the knowledge of the three dimensional atomic structure of each members' SH2 domain. Here we present the solution structure of the hGrb7-SH2 domain in complex with a 10 amino acid peptide representing the binding site on the erbB2 receptor (pY1139, PQPEpYVNQPD). The general topology of an SH2 domain with an N-terminal α-helix, a central β-sheet region and a C-terminal α-helix has been elucidated, as well as the four amino acid insertion in the region between the βE strand and the EF loop shown to be involved in binding with the ligand. Our structure reveals the bound pY1139 peptide in a β-turn conformation, similar to the Shc-derived phosphotyrosine-containing peptide in complex with the Grb2 SH2 domain (Ogura et al., 1999).

Materials and methods

Sample preparation

The pGEX-2T expression plasmid containing the hGrb7-SH2 gene insert (R. Daly, Janes et al., 1997) was transformed into *Escherichia coli* BL21(DE3) cells and expressed at 37 °C (310 K). The SH2 domain, consisting of residues 435–536 of the hGrb7 protein, was expressed as a Glutathione S-Transferase (GST) fusion protein and was purified by standard protocols (Guan and Dixon, 1991). The fusion protein was bound to Glutathione Sepharose beads, the impurities washed away, and the SH2 domain released from the immobilized GST protein through the utilization of a thrombin cleavage site. Typical yields of pure hGrb7-SH2 were 5–6 mg per liter of culture. Uniformly ^{15}N-labeled protein was produced in minimal media containing 1 g l^{-1} $(^{15}NH_4)_2SO_4$ (Cambridge Isotope Labs, Woburn, MA, U.S.A.). Uniformly ^{13}C and ^{15}N double labeled protein was produced in the same media containing 2 g l^{-1} [$^{13}C_6$]-D-glucose (Cambridge Isotope Labs). The NMR samples were prepared in an acetate buffer at pH 6.6 containing 100 mM NaCl, 52.2 mM CH_3COOH, 5 mM DTT, 1 mM EDTA, 0.9 mM NaN_3 and 90% H_2O/10% D_2O. The hGrb7-SH2 protein concentrations of the samples were 0.6 to 0.8 mM and the pY1139 peptide was added in a 1:1 stoichiometric ratio as previously described (Brescia et al., 2002).

NMR spectroscopy

All NMR spectra were recorded at a temperature of 298 K on a Varian INOVA 500 MHz spectrometer equipped with a ^{1}H/^{13}C/^{15}N probe and Z-axis pulsed field gradient capabilities. Table 1 summarizes the acquisition parameters for the NMR experiments used in determining the solution structure of hGrb7-SH2 in complex with pY1139. Previously reported (Brescia et al., 2002) 2D and 3D homonuclear and heteronuclear experiments were also used and included in the table for completeness. Solvent suppression was achieved using pulsed field gradient coherence selection and on-resonance low-power presaturation of the water signal during the relaxation delay. Quadrature detection in the phase sensitive mode was achieved by the method of States-TPPI (Marion et al., 1989). Spectra were processed on Silicon Graphics workstations using the Azara 2.6 software package (Wayne Boucher, University of Cambridge). Standard processing in all dimensions included zero filling to the next power of 2 followed by multiplication by a phase shifted sine bell curve. All spectra were referenced to external TSP (0.0 ppm) in the ^{1}H dimension. The ^{13}C and ^{15}N chemical shifts were referenced indirectly to TSP using the ratios 0.251449530 and 0.101329118, respectively, for the zero-point frequencies (Wishart et al., 1995).

Uniformly ^{15}N-labeled hGrb7-SH2/pY1139 was used to collect 2D ^{1}H-^{15}N HMQC-J spectra (Forman-Kay et al., 1990; Kay and Bax, 1990) at 500 MHz using States-TPPI quadrature detection. The same sample was used to record the 3D ^{1}H-^{15}N NOESY-HSQC (Kay et al., 1992; Zhang et al., 1994) and the 3D ^{1}H-^{15}N TOCSY-HSQC (Zhang et al., 1994). Uniformly ^{15}N- and ^{13}C-labeled hGrb7-SH2/pY1139 was used to collect the 3D ^{13}C-^{15}N NOESY-HSQC, ^{13}C-NOESY-HSQC (Clore et al., 1991; Kay, 1995) and various 2D ^{15}N and ^{13}C isotope filtered spectra (Otting and Wüthrich, 1990) at 500 MHz using States-TPPI quadrature detection. A representative carbon resonance plane of the ^{13}C edited three dimensional NOESY spectrum is shown in Figure 1, and a small portion of the two dimensional ^{15}N-^{13}C F2-filtered NOESY (^{13}C, ^{15}N $\rightarrow$ ^{12}C, ^{14}N NOESY) spectrum showing representative NOE interactions between the pY1139 peptide and the hGrb7-SH2 domain is seen in Figure 2.

Resonance assignments

The majority of the resonances in the spectra of pY1139 bound to hGrb7-SH2 domain have been previously assigned (Brescia et al., 2002). All non-exchangeable side chain resonances were assigned using various 2D and 3D homonuclear and heteronuclear spectra including: ^{1}H-^{15}N NOESY-HSQC, ^{1}H-^{15}N TOCSY-HSQC, HCCH-TOCSY, ^{1}H-^{13}C NOESY-HSQC, and ^{15}N-HSQC. Resonance assignments of the phosphorylated erbB2 peptide pY1139 were achieved through analysis of a combination of heteronuclear ^{15}N and ^{13}C isotope filtered TOCSY and NOESY experiments (Otting and Wüthrich, 1990). The assignments were performed using the interactive graphics program ANSIG for Windows v1.0 (Helgstrand et al., 2000).

Structure calculations

NOE distance integration was done using ANSIG 3.3 (Kraulis, 1989; Kraulis et al., 1994) on Silicon Graphics workstations using box summation integration (very weak 1.8–6 Å, weak 1.8–5 Å, medium

Table 1. Parameters used in NMR experiments

Experiment	Dimension	Nucleus	Time points	Frequency points	Acquisition time	Carrier frequency
CN NOESY-HSQC	t_1	^{13}C	32	64	3.56 ms	43 ppm
	t_2	^{1}H	128	128	15.04 ms	4.7 ppm
	t_3	^{1}H	1024	1024	60.16 ms	4.7 ppm
3D NOESY-HSQC	t_1	^{15}N	16	128	7.27 ms	120 ppm
	t_2	^{1}H	64	256	10.67 ms	4.7 ppm
	t_3	^{1}H	1024	1024	64 ms	4.7 ppm
3D NOESY-HSQC	t_1	^{13}C	32	64	3.56 ms	43 ppm
	t_2	^{1}H	96	256	11.28 ms	4.7 ppm
	t_3	^{1}H	1024	1024	60.16 ms	4.7 ppm
3D TOCSY-HSQC	t_1	^{1}H	32	64	14.54 ms	119 ppm
	t_2	^{1}H	64	128	7.53 ms	4.7 ppm
	t_3	^{15}N	1024	1024	60.16 ms	4.7 ppm
2D HMQC-J	t_1	^{15}N	1024	2048	465.5 ms	119 ppm
	t_2	^{1}H	1024	1024	60.16 ms	4.7 ppm
2D HSQC	t_1	^{15}N	128	512	64 ms	119 ppm
	t_2	^{1}H	1024	1024	60.16 ms	4.7 ppm
3D HNCA	t_1	^{15}N	16	32	3.81 ms	119 ppm
	t_2	^{13}C	64	128	14.5 ms	56 ppm
	t_3	^{1}H	1024	1024	51.2 ms	4.7 ppm
3D HNCOCA	t_1	^{15}N	16	32	7.27 ms	120 ppm
	t_2	^{13}C	64	128	14.5 ms	56 ppm
	t_3	^{1}H	1024	1024	51.2 ms	4.7 ppm
3D CBCACONH	t_1	^{15}N	16	32	7.27 ms	120 ppm
	t_2	^{13}C	53	128	5.86 ms	46 ppm
	t_3	^{1}H	1024	1024	51.2 ms	4.7 ppm
3D HNCACB	t_1	^{15}N	16	32	7.27 ms	120 ppm
	t_2	^{13}C	64	128	7.07 ms	46 ppm
	t_3	^{1}H	1024	1024	51.2 ms	4.7 ppm
3D CBCANH	t_1	^{15}N	16	32	7.27 ms	120 ppm
	t_2	^{13}C	53	128	5.86 ms	46 ppm
	t_3	^{1}H	1024	1024	51.2 ms	4.7 ppm
3D HCCH-TOCSY	t_1	^{13}C	32	64	3.55 ms	35 ppm
	t_2	^{1}H	128	128	15.04 ms	4.7 ppm
	t_3	^{1}H	1024	1024	60.16 ms	4.7 ppm
$^{13}C, ^{15}N \rightarrow {}^{12}C, {}^{14}N$	t_1	^{1}H	128	512	16 ms	3.0 ppm
NOESY	t_2	^{1}H	1024	1024	64 ms	3.0 ppm
$^{12}C, ^{14}N \rightarrow {}^{13}C, {}^{15}N$	t_1	^{1}H	256	512	34.13 ms	3.0 ppm
NOESY	t_2	^{1}H	1024	1024	68.18 ms	3.0 ppm
$^{12}C, ^{14}N \rightarrow {}^{12}C, {}^{14}N$	t_1	^{1}H	128	512	15.06 ms	3.0 ppm
NOESY	t_2	^{1}H	1024	1024	60.16 ms	3.0 ppm
$^{12}C, ^{14}N \rightarrow {}^{12}C, {}^{14}N$	t_1	^{1}H	256	512	30.1 ms	3.0 ppm
TOCSY	t_2	^{1}H	1024	1024	60.16 ms	3.0 ppm

1.8–3.3 Å, strong 1.8–2.7 Å). Short and medium range NOE connectivity patterns for the hGrb7-SH2 domain are available as supplementary material. The distance restraints were directly output into XPLOR format after scaling of methyl intensities, ignoring crosspeaks reflecting trivial distances and addition of pseudoatom distance correction for nonstereo assigned groups. A total of 62 hydrogen bond restraints were employed, assigned based upon evaluation of candidate hydrogen bonds calculated in the absence of hydrogen bond

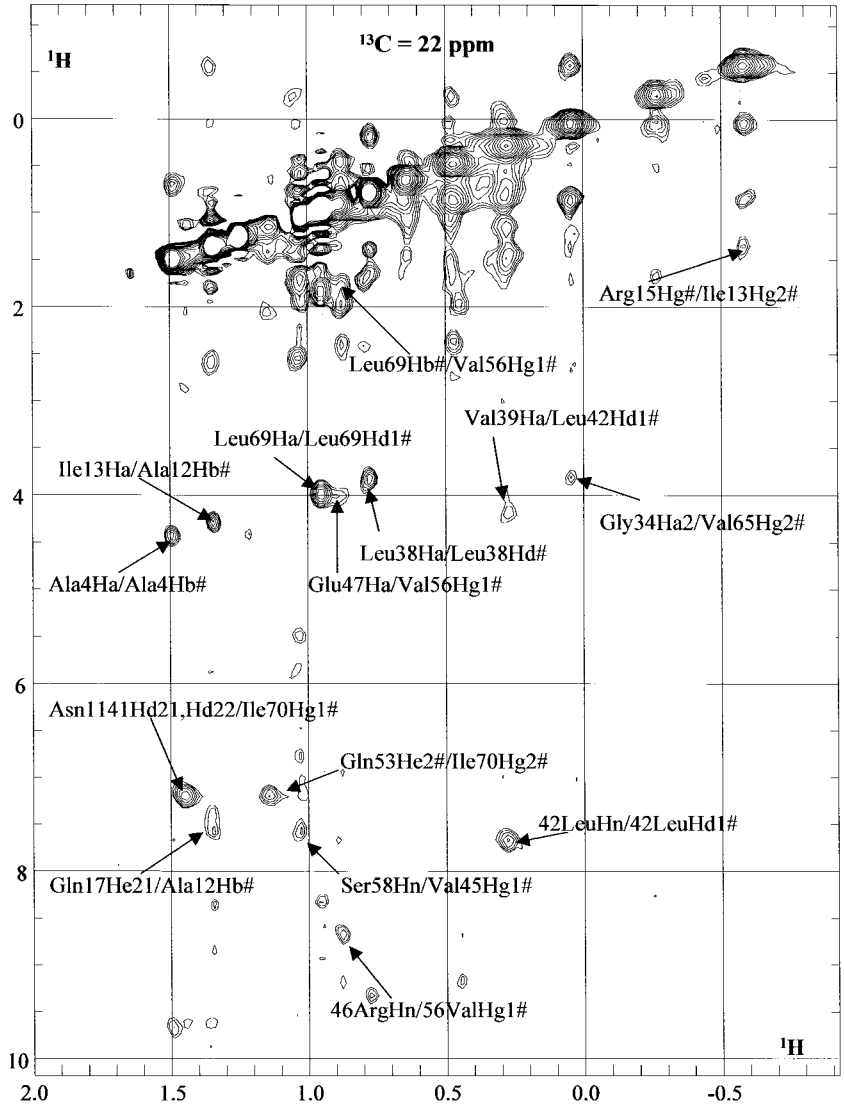

Figure 1. A representative carbon frequency plane (^{13}C = 22 ppm) of the ^{13}C edited three dimensional NOESY spectrum is shown. Representative nOe interactions are labeled as for example: 47GluHa/56ValHg1# represents the nOe interaction seen between the 47Glu alpha proton in the y-axis and the 56Val gamma−1 protons in the x-axis. Many intra-residue and sequential residue interactions are not shown labeled for the sake of clarity. Acquisition parameters are listed in Table 1.

restraints, coupled with backbone NOE patterns and chemical shifts. An exception includes three hydrogen bonds defining the phosphotyrosine phosphate stabilization by two conserved arginine residues (Arg 26 and Arg 46) and one conserved serine residue (Ser 48). These hydrogen bonds were explicitly included as constraints in the original structure calculations. This was based upon observed NOE constraints between the pTyr 1139 aromatic ring and the SH2 domain, as well as the phosphotyrosine hydrogen bonding stabilization patterns documented in previous SH2 domain structures in the literature (Waksman et al., 1993; Pascal et al., 1994; Ogura et al., 1999). These hydrogen bonds are: pTyr 1139 phosphate oxygen to Arg 46 ηN-H protons, pTyr 1139 phosphate oxygen to Arg 26 ηN-H protons and pTyr 1139 phosphate oxygen to the Ser 48 γO-H proton. They were introduced in an ambiguously assigned manner, allowing the observed NOE constraints to drive the final orientation of the pTyr 1139 phosphate within the phosphotyrosine binding pocket. Structure calculations performed *without* these explicit hydrogen bonds result in structures with

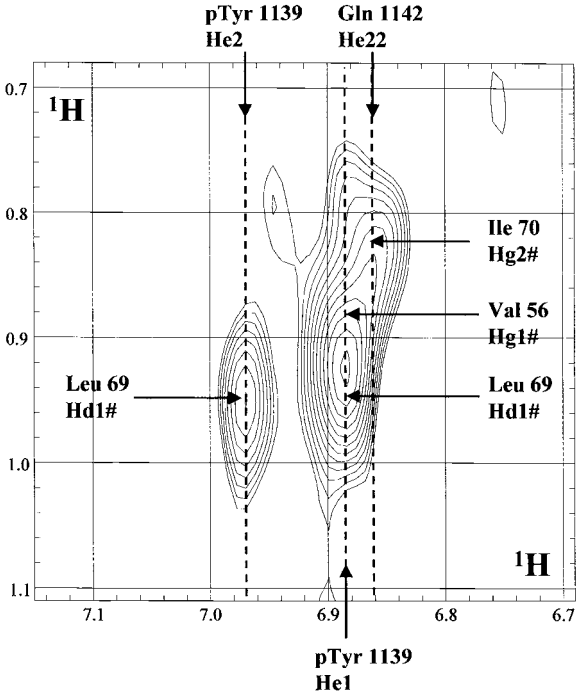

Figure 2. A small portion of the two dimensional ^{15}N-^{13}C F2-filtered NOESY (^{13}C, ^{15}N $\rightarrow$ ^{12}C, ^{14}N NOESY) spectrum displaying representative NOE interactions between the pY1139 peptide and the hGrb7-SH2 domain is shown. Labeling is such that the F2 (x-axis) labels represent peptide proton resonances, and F1 (y-axis) labels represent SH2 domain proton resonances. Acquisition parameters are listed in Table 1.

the same hydrogen bonding patterns to the phosphate present, but in a more intermittent manner.

The final structure calculation was based on a total of 1660 distance constraints, of which 655 were intra-residue, 475 sequential, 172 medium range and 358 long range as listed in Table 2. The numbers and distribution of NOE-derived distance constraints along the sequence of hGrb7-SH2 are available as supplementary material. Dihedral angle constraints for backbone ϕ angles were derived from NOE patterns, $^3J_{HN-H\alpha}$ couplings measured from 2D HMQC-J experiments with an extended t_1 acquisition time (Kay and Bax, 1990) and Cα and Cβ chemical shift conformational dependencies (Kuszewski et al., 1995).

Characterization of this peptide in the bound state involved the inclusion of 5 intra-residue NOEs, 10 sequential NOEs, 8 medium range within-peptide NOEs and 57 long range peptide-to-SH2 domain NOEs into the final structure calculations. The NOE constraints specific to the erbB2 pY1139 phosphorylated peptide are available as supplementary material.

The structures were calculated using the program Crystallography and NMR System (CNS) version 1.1 (Brünger et al., 1998). Structure calculations were performed starting from extended structures in torsion angle space dynamics followed by Cartesian minimization. An initial high temperature stage was performed at a temperature of 50 000 K and included 1000 molecular dynamics steps of 15 fs each. The first slow cooling stage consisted of 2000 steps of 3.8 fs each, with temperature annealing from 50 000 K to 0 K during this stage. The second slow cooling stage consisted of 12 000 steps of 0.13 fs each and temperature annealing from 2000 K to 0 K. The Cartesian energy minimization consisted of 4000 steps, with the final values for the force constants of 400 kcal mol^{-1} rad^{-2} for angles and improper torsions and 75 kcal mol^{-1} Å^{-4} for experimental distance restraints. The summary of the statistics for the final ten structures is listed in Table 2.

Results and discussion

Grb7-SH2 domain structure

The NMR solution structure of the SH2 domain of human Grb7 in complex with the erbB2 phosphorylated peptide pY1139 was solved using three-dimensional heteronuclear ^{15}N- and ^{13}C-edited NOESY and isotope filtered NOESY NMR experiments. The root-mean-square deviation (RMSD) for the ten representative structures is 0.73 Å for the backbone heavy atoms of residues 17 through 116 of the SH2 domain, and residues 1139 through 1142 of the pY1139 peptide. The RMSD for the same residues of the SH2 domain and erbB2 peptide including all atoms is 1.14 Å. The hGrb7-SH2 structure (Figure 3), with its three long anti-parallel β strands (βB, βC and βD), flanked by a few smaller β strands (βE and βF), and an α helix at each end (αA and αB) reveals the standard SH2 domain structure. An exception is the βE strand which is one residue longer than the classic SH2 domain βE strand. This extension is part of a four amino acid insert in this region typical for this family of proteins that elongates the EF loop by three residues, and corresponds to a region of the domain that often interacts with the pTyr +3 residue in ligand binding (Waksman et al., 1993). The locations of the secondary structural elements of the hGrb7-SH2 domain are presented schematically in Figure 4. Three short β-strands known to occur in other SH2 domain

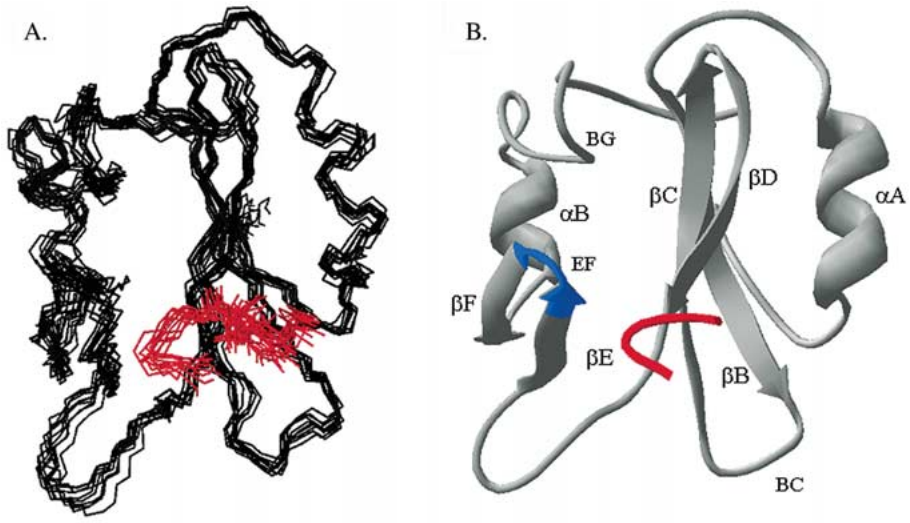

Figure 3. Solution structure of the human Grb7-SH2 domain in complex with the erbB2 representative phosphorylated peptide pY1139. The hGrb7-SH2 domain is represented in black/grey and the pY1139 peptide is shown in red. (A) Overlay of ten representative calculated structures as described in the text. The backbone trace is shown for each structure. Residues 1–16 and 117–120 of the SH2 domain and 1135–1138 and 1143–1145 of the peptide are not visualized, and are primarily unstructured due to a lack of observable inter-residue NOE interactions. (B) Ribbon representation of a single structure selected from the ten overlaid structures in A. Secondary structural elements are labeled from the N-terminus to the C-terminus, with αA being the N-terminal α helix, αB the C-terminal α-helix, etc. following the nomenclature of Eck et al. (1993). The location of the insertion residues is indicated in blue. Although β-strand A is not seen in the representative structure it is present in approximately half the structures calculated. Graphical representation of the hGrb7-SH2 domain and the pY1139 peptide was achieved using the software SWISSPDB viewer (Guex and Peitsch, 1997).

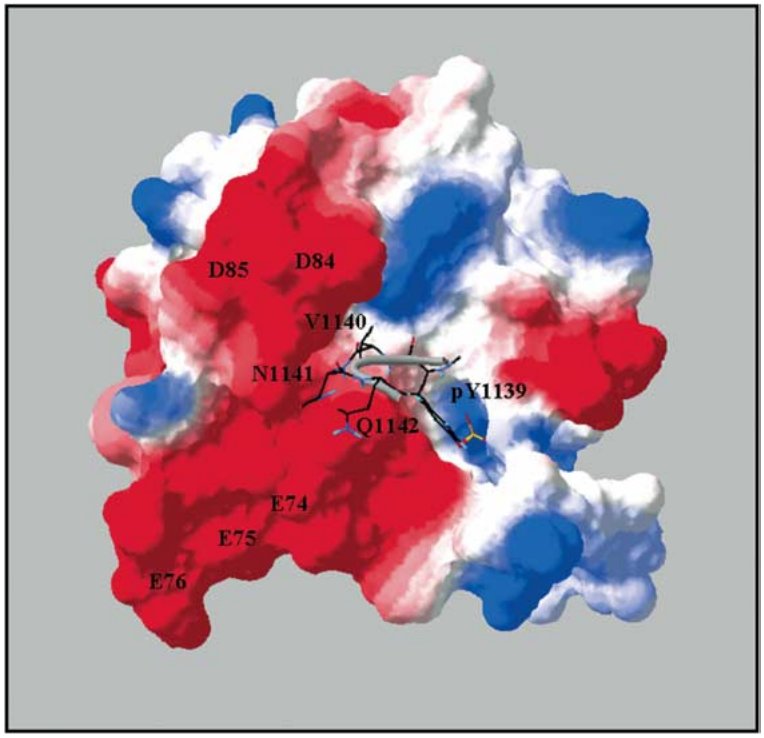

Figure 5. Molecular surface of the hGrb7-SH2 domain in complex with pY1139 shown in approximately the same orientation as in Figure 3. The surface electrostatic potential is shown in red (negative), blue (positive) and white (neutral). The approximate locations of the acidic residue sidechains of Asp 84, Asp 85, Glu 74, Glu 75 and Glu 76 are indicated. The figure was prepared using the program SWISSPDB viewer.

Table 2. Summary of statistics for the 10 final structures

NOE upper distance limits	1660
Intra-residue	655
Sequential	475
Medium-range	172
Long-range	358
Dihedral angle constraints	120
Hydrogen bonds	2×62
R.M.S.D. from experimental constraints	
Distances (Å)	0.0904 ± 0.0108
Dihedrals (°)	0.9457 ± 0.0454
Average number of NOE distance constraint violations	
> 0.5 Å	0.40 ± 0.843
> 0.2 Å	7.70 ± 2.946
R.M.S.D. from idealized covalent geometry	
Bonds (Å)	0.0048 ± 0.00014
Angles (°)	0.9159 ± 0.0159
Impropers (°)	1.1548 ± 0.0193
Atomic R.M.S.D. values (Å)	
SH2 domain residues 17–116 and pY1139 peptide residues 1139–1142	
Backbone atoms	0.73 Å
All atoms	1.14 Å
Ramachandran plot (%)[a], residues 1 to 120	
Most favored regions	56.5%
Additional allowed regions	38.9%
Generously allowed regions	4.6%
Disallowed regions	0.0%

[a]For the chosen representative structure of the ensemble and excluding all glycines and prolines.

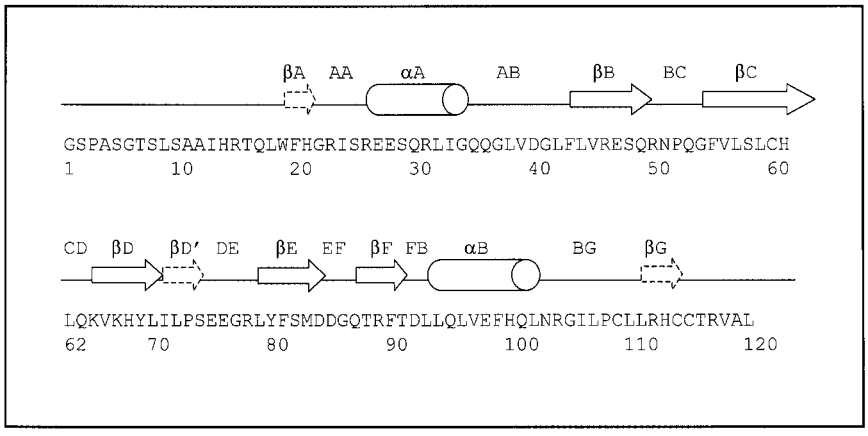

Figure 4. Sequence and secondary structural elements for the hGrb7-SH2 domain in complex with pY1139.

structures, βA, βD′ and βG, are not observed in the representative hGrb7-SH2/pY1139 complex structure presented. Although the ϕ/ψ angles for the residues in these regions are close to β-strand values, the criteria for canonical β conformation are met for only two consecutive residues in each case. Therefore the βA, βD′ and βG strands can be considered to be present, in abbreviated form. The location of these β-strands is indicated by dotted-line arrows in Figure 4. The Ramachandran plot analysis of a selected representative structure yields 56.5% of residues falling within the most favored region, 38.9% within an additionally allowed region, 4.6% within a generously allowed region, and 0.0% within the disallowed region. This analysis is performed excluding the proline, glycine and terminal residues as determined by the program ProCheck (Laskowski et al., 1993).

The backbone traces of the final ten representative hGrb7-SH2 domain/pY1139 peptide solution structures are shown in Figure 3A. A single representative structure of the ten is shown in a ribbon representation (Figure 3B) and used for discussion of observed hydrogen bonding patterns in the remainder of the manuscript. The hydrogen bonding patterns observed in the representative structure are seen in the overwhelming majority of the calculated structures, and do not deviate significantly from calculation to calculation. The human Grb7-SH2 domain has the same overall fold as that of the numerous other published SH2 domain structures (Booker et al., 1992; Waksman et al., 1993; Pascal et al., 1994; Thornton et al., 1996; Wang et al., 1996). The hGrb7-SH2 domain shares 33% amino acid identity with the vSrc-SH2 domain and 29% amino acid identity with the Grb2-SH2 domain. Molecular alignment of the hGrb7-SH2 domain structure with a representative vSrc-SH2 domain structure (Waksman et al., 1993) and Grb2-SH2 domain structure (Wang et al., 1996) gives a backbone atom RMSD of 3.6 Å and 3.4 Å, respectively.

The insertion region between the βE strand and the EF loop, specifically residues Met 83 through Gly 86, appears to result in the C-terminal α-helix (αB) tilting slightly back, so that the αB helix is in the same plane as the αA helix. In both vSrc-SH2 and Grb2-SH2 domain structures, the αB helix is tilted slightly forward towards the EF loop and out of the plane defined by the central β-sheet and N-terminal α-helix, αA (Waksman et al., 1993; Ogura et al., 1999; Wang et al., 1996). The hydrophobic pocket that normally accepts the +3 hydrophobic residue of the phosphorylated peptide during binding is not apparent. Instead the EF loop region is in a 'closed' conformation, with the region between the loop and the rest of the SH2 domain closely packed by the hydrophobic sidechains of residues Leu 57, Leu 59, Tyr 68, Met 83, Ile 106, Leu 107 and Val 1140 (+1 residue) of the erbB2 peptide. When the structure of vSrc-SH2 domain in complex with the peptide pYEEI (Waksman et al., 1993) is aligned with the hGrb7-SH2/pY1139 complex structure, the position normally occupied by the +3 Ile residue of pYEEI has a high negative overall charge due to the hGrb7-SH2 domain Asp 84 and Asp 85 sidechains (Figure 5).

Comparing the hGrb7-SH2/pY1139 complex structure to the Grb2-SH2/Shc pTyr peptide complex (Ogura et al., 1999) reveals that the insertion residues (Met 83 through Gly 86) in the EF loop of the hGrb7-SH2 domain occupy the position of the Trp 66 sidechain in the EF loop of the Grb2-SH2 domain (Figure 6). Although the two SH2 domains do not share amino acid identity in this region, the function associated with the EF loop appears to be similar between the two. In the Grb2-SH2 domain, the bulky Trp 66 residue results in the Shc pTyr peptide adopting a β-turn conformation, while in the hGrb7-SH2 domain, the four amino acid insertion results in the pY1139 adopting this same conformation. Thus, the EF loop in both Grb2 and Grb7 determines the binding conformation of the peptide. As previously stated, the hGrb7 SH2 domain structure and the Grb2 SH2 domain structure (Wang et al., 1996) are very similar, with backbone atom RMSD of 3.4 Å and the main structural differences located in the insertion region of the EF loop and the tilt of the αB helix.

The lack of a hydrophobic pocket available for binding the +3 residue of phosphopeptides seen in the hGrb7-SH2/pY1139 complex structure is consistent with the recently determined X-ray crystal structure of the Grb10-SH2 domain (Stein et al., 2003). In the Grb10-SH2 domain structure, residues in the BG and EF loops are positioned to interfere with potential binding of the +3 residue in the phosphotyrosine peptide ligands.

ErbB2 peptide conformation

Through single and double isotope filtered NOESY experiments the bound conformation of pY1139 in complex with the hGrb7-SH2 domain has been elucidated. A total of 80 NOE interactions have been interpreted both within the peptide itself and between the peptide and the SH2 domain. The 57 peptide-

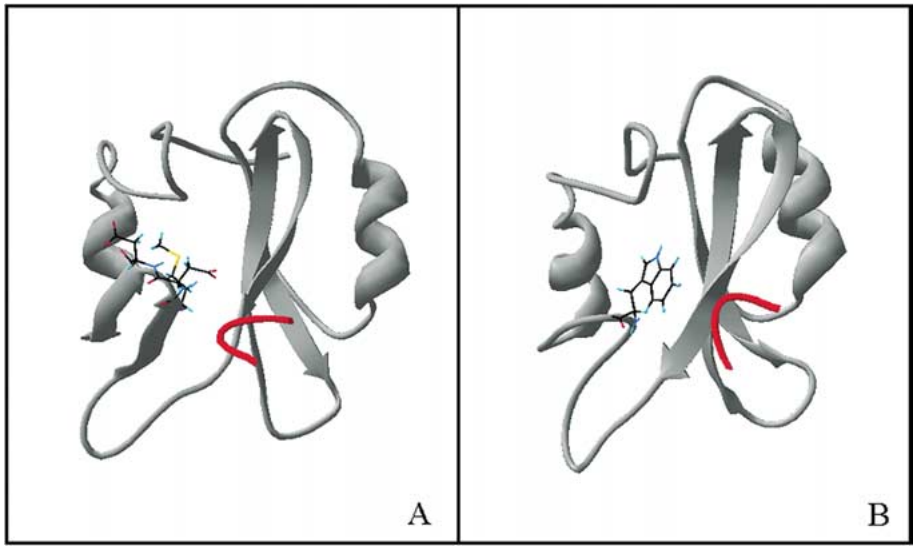

Figure 6. Graphical comparison between the hGrb7-SH2/pY1139 complex structure and the Grb2-SH2/Shc peptide structure (Ogura et al., 1999). For the displayed residues oxygen atoms are shown in red, nitrogen atoms in dark blue, carbon atoms in white and hydrogen atoms in light blue. (A) The same representative structure as in Figure 3 is shown of the hGrb7-SH2/pY1139 complex. The sidechains of residues Met 83, Asp 84 and Asp85 are visualized to emphasize their location with respect to the corresponding region of the Grb2-SH2 domain. (B) The Grb2-SH2 domain in complex with a Shc derived phosphopeptide is shown at approximately the same orientation as the hGrb7-SH2/pY1139 complex structure in A. The Trp 66 sidechain is visualized to emphasize its similar location with respect to the insertion region in the hGrb7-SH2 domain. The figure was prepared using the program SWISSPDB viewer.

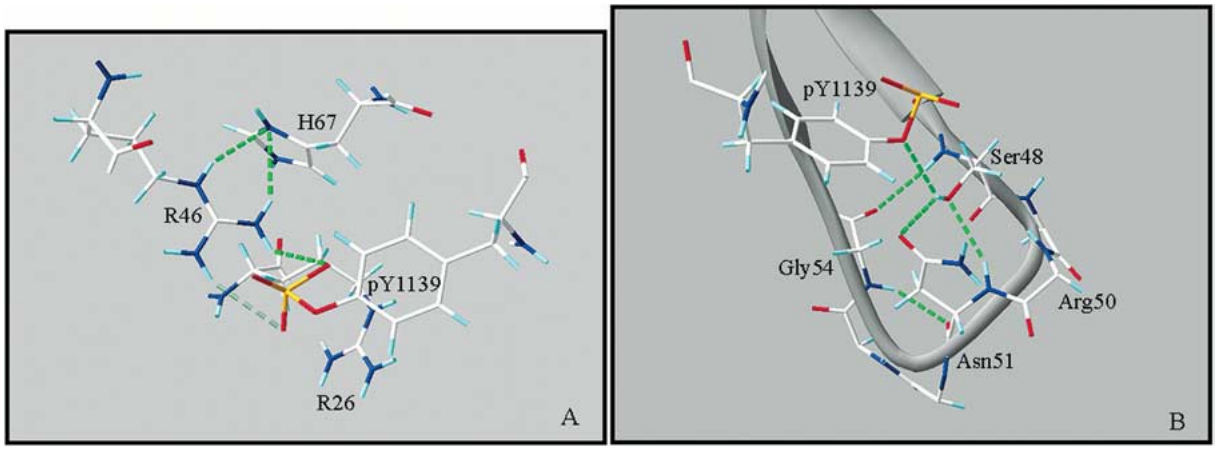

Figure 7. Observed hydrogen bonding patterns in the phosphotyrosine coordination region of a representative hGrb7-SH2 domain/pY1139 structure. Oxygen atoms are shown in red, nitrogen atoms in dark blue, carbon atoms in white and hydrogen atoms in light blue. The pTyr 1139 phosphate oxygen hydrogen bonds with the Arg 46 sidechain η hydrogens and Ser 48 γ hydrogen are included explicitly in the structure calculations. Structure calculations performed *without* these explicit hydrogen bonds result in structures with the same hydrogen bonding patterns. (A) pTyr 1139 phosphate oxygen interactions with the Arg 46 sidechain η hydrogens, His 67 sidechain δ nitrogen interactions with the Arg 46 sidechain ε and η hydrogens; (B) pTyr 1139 phosphate oxygen and Ser 48 γ proton, Asn 51 sidechain δ oxygen and the Ser 48 γ proton, Ser 48 γ oxygen with the Arg 50 amide proton, Ser 48 amide hydrogen and the Gly 54 carbonyl oxygen. The figure was prepared using the program SWISSPDB viewer.

to-protein domain NOE interactions provide ample constraints to dock the peptide on the SH2 domain as well as determine the erbB2 peptide bound conformation itself. Multiple NOE interactions are observed between residues 81 through 84 (Phe 81, Ser 82, Met 83 and Asp 84) and the pY1139 peptide +1 and +2 residues (Val 1140 and Asn 1141).

A strong NOE interaction is observed between the +1 valine residue (Val 1140) α proton and the +3 glutamine (Gln 1142) α proton. Another intermediate strength NOE is observed between the Val 1140 amide proton and the +4 residue (Pro 1143) α proton. Through these and other protein to peptide observed NOE interactions, the pY1139 peptide is shown to be in a tight β-turn composed of primarily three residues, Val 1140, Asn 1141 and Gln 1142. Contacts between the pY1139 peptide and the SH2 domain discussed below hold residues pTyr 1139 through Gln 1142 in a well defined conformation. The rest of the phosphorylated peptide residues, consisting of Pro 1135 through Glu 1138 and Asp 1144, have no constrained conformation.

Interactions between the hGrb7-SH2 domain and the ErbB2 peptide

Coordination of the pTyr phosphate by hGrb7 mirrors the pattern of primarily ionic stabilization seen in other SH2 domain/phosphorylated peptide complexes (Waksman et al., 1993; Pascal et al., 1994; Ogura et al., 1999). Highly conserved residues βB5 (Arg 46 in hGrb7-SH2), αA2 (Arg 26 in hGrb7-SH2) and BC1 (Ser 48 in hGrb7-SH2) line the phosphotyrosine binding pocket and are in favorable orientations to allow stabilization of the pTyr 1139 phosphate to occur (Figure 7A). The Arg 46 sidechain η hydrogen is only visible in the ^{15}N-HSQC spectrum of the hGrb7-SH2/pY1139 complex, and not in the ^{15}N-HSQC spectrum of free hGrb7-SH2 domain. This experimental evidence suggests that this hydrogen is involved in a hydrogen bond only when the phosphopeptide is present. Arg 46 is further involved in a hydrogen bonding network with a highly conserved residue at position βD4 (His 67). The sidechain γ oxygen of Ser 48 is in a hydrogen bonding pattern to the backbone amide proton of Asn 51. Ser 48 has an additional hydrogen bond between its sidechain γ proton and the sidechain carbonyl oxygen of Asn 51 (Figure 7B). This could explain the large observed chemical shift change in the Asn 51 backbone amide resonance upon peptide binding (Brescia et al., 2002). Coordination of Asn 51 with the pTyr phosphate through Ser 48 likely necessitates an appreciable conformational change. A similar argument can be made for the largest chemical shift seen upon binding the pY1139 peptide for any of the glycine residues of hGrb7-SH2, Gly 54. This residue is in an appropriate orientation to allow formation of a hydrogen bond between the Ser 48 amide proton and the Gly 54 carbonyl oxygen (Figure 7B).

Residues Tyr 68 and Leu 69 at positions βD5 and βD6 have been shown to determine hGrb7-SH2 binding to the erbB2 peptide pY1139 (Janes et al., 1997). In the hGrb7-SH2/pY1139 complex Tyr 68 is in close contact with the +1 valine residue (Val 1140) methyl groups of the pY1139 peptide (Figures 8A and 8B). The closest Val 1140 methyl group is an average distance of 3.3 Å from the Tyr 68 aromatic ring, thus it is likely the two residues are involved in a hydrophobic stabilizing interaction. The Tyr 68 hydroxyl is further hydrogen bonded to the backbone carbonyl of Leu 107 in the BG loop. In the Grb2-SH2 domain (Ogura et al., 1999) the corresponding residues Phe 53 (βD5) and Ile 85 (in the BG loop) engage in a simple hydrophobic packing interaction, since Phe 53 has no hydroxyl group available for hydrogen bonding. Tyr 68 appears to provide a pivotal stabilizing role in the hydrophobic packing of not only the +1 valine residue of pY1139 but for the region of the SH2 domain defined by the EF loop, αB helix, and BG loop. Van der Waals contacts are seen between the aromatic ring of Tyr 68 and the methyl/methylene groups of the following residues in this region: Leu 57, Leu 59, Met 83, Ile 106 and Leu 107. In the same manner, Leu 69 (βD6) is in close contact with the phosphorylated tyrosine aromatic ring of pY1139 (Figures 8A and 8B). The average distance between the Leu 69 methyl groups and the pTyr 1139 aromatic ring is 3.2 Å, which allows favorable hydrophobic interactions to occur. Speculation on the importance of these contacts in determining Grb7 binding specificity is discussed later in this manuscript.

The +2 asparagine residue of the erbB2 peptide (Asn 1141) is primarily solvent exposed. Exceptions are seen in close contacts between the asparagine sidechain carbonyl and the Ser 82 sidechain hydroxyl proton, which form a hydrogen bond in many of the calculated structures (Figure 8C). The corresponding residue in the Grb2-SH2/pYINQ complex structure (Rahuel et al., 1998) is a leucine (Leu 65). Leu 65 of Grb2-SH2 immediately precedes the tryptophan residue (Trp 66) responsible for the bound turn

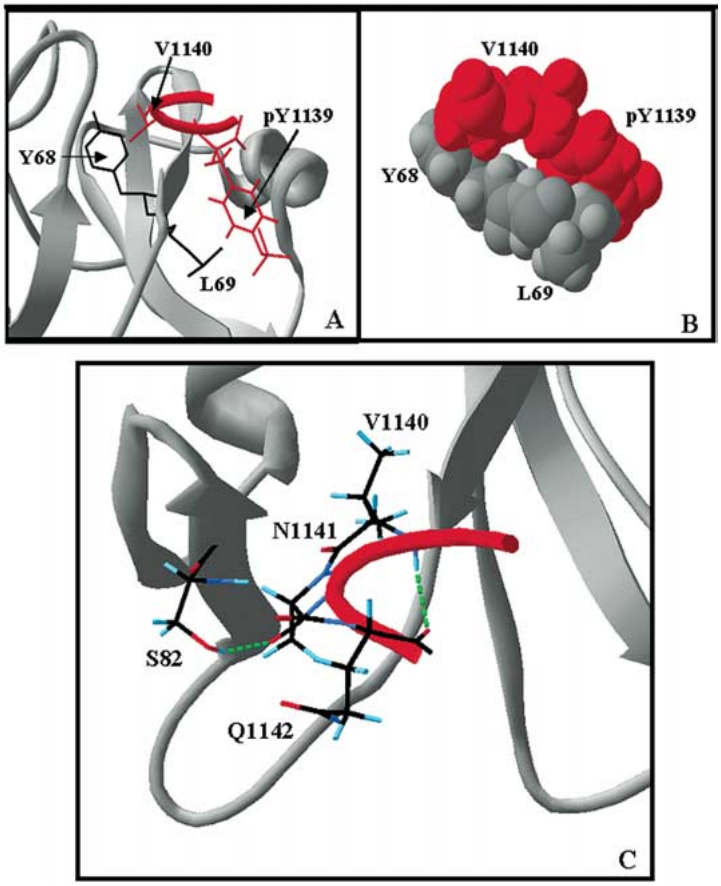

Figure 8. Observed non-phosphate related interactions between the hGrb7-SH2 domain and the pY1139 peptide in a representative hGrb7-SH2 domain/pY1139 structure. (A) Hydrophobic packing interactions between Val 1140 of the peptide and Tyr 68 of the SH2 domain, and between the pTyr 1139 aromatic ring of the peptide and Leu 69 of the SH2 domain. The pY1139 peptide residues are shown in red and the hGrb7-SH2 domain residues are shown in black; (B) space-filled representation of the same interaction seen in A; and (C) observed hydrogen bonding pattern between the peptide Asn 1141 sidechain carbonyl oxygen and the Ser 82 sidechain hydroxyl proton. An additional *intra*-peptide hydrogen bond is seen between the Gln 1142 backbone carbonyl oxygen and the Val 1140 amide hydrogen. Oxygen atoms are shown in red, nitrogen atoms in dark blue, carbon atoms in black and hydrogen atoms in light blue. The figure was prepared using the program SWISSPDB viewer.

conformation of Grb2-SH2 peptide ligands, whereas Ser 82 of hGrb7-SH2 immediately precedes the four residue insertion between the βE strand and the EF loop. In Grb2-SH2/phosphopeptide complex structures a hydrogen bond is formed between the carbonyl oxygen of Leu 65 and the peptide +2 asparagine sidechain amide proton (Rahuel et al., 1998; Ogura et al., 1999). This orientation places the asparagine sidechain carbonyl in a favorable position to form hydrogen bonds to the amide hydrogen of the βD6 residue (Lys 54) in the Grb2-SH2 domain. The orientation of the +2 Asn 1141 residue in the hGrb7-SH2/pY1139 complex makes the formation of hydrogen bonds between the SH2 domain βD6 residue Leu 69 and Asn 1141 less likely, since greater distances exist between the potentially interacting functional groups.

The importance of the +3 position in pY1139, Gln 1142, is not fully elucidated in the hGrb7-SH2/pY1139 complex structure. Fiddes et al. (1998) have demonstrated that the +3 position to the phosphotyrosine is of some importance in Grb7 and Grb2 binding to erbB2 (+3 position = Gln) and/or erbB3 (+3 position = Arg) representative phosphopeptides. However, in that study mutation of this residue provided conflicting results, so that a trend for the effect of glutamine versus arginine at this position could not be established in understanding Grb7 versus Grb2 specificity. As discussed in the introduction, the Grb14-SH2 domain will *not* bind to pY1139, the

erbB2 representative peptide containing a pYVNQ sequence. Mutations at either the βD5 or βD6 position to the corresponding hGrb7-SH2 domain residues (βD5:F/Y;βD6:Q/L) result in a Grb14-SH2 domain mutant that binds pY1139 (Janes et al., 1997). The βD5 position is a site which often interacts with the +1 and the +3 residues subsequent to the phosphotyrosine (Lovell et al., 2000; Choi et al., 2001). In the Grb7-SH2/pY1139 structure presented, the +1 valine residue of pY1139 has extensive hydrophobic contacts with the βD5 Tyr 68 residue (Figures 8A and 8B), and is likely important in the specific binding of erbB2. In contrast to other SH2 domains, the +3 residue (Gln 1142) has no direct contact with the βD5 residue or with any part of the SH2 domain, except through minimal van der Waals contacts between its methylene groups and the βD7 (Ile 70) δ-methyl group. However, calculation of the electrostatic potential surface of the hGrb7-SH2 domain demonstrates the polar Gln 1142 sidechain rests over a highly electronegative region of the SH2 domain (Figure 5). This may contribute additional stabilizing interactions responsible for the preference of hGrb7-SH2 for a Gln/Arg residue in the +3 position subsequent to the phosphotyrosine in its binding partners.

The overall highly electronegative nature of the hGrb7-SH2 domain molecular surface is striking, and is primarily a result of conserved Asp and Glu residues in the βD strand, βE strand and EF loop regions in this protein family. Despite the proximity of this negative potential to the phosphopeptide binding site, the observed NOE interactions between the peptide and the SH2 domain indicate the +1 residue Val 1140 is held firmly in place between residues Asp 84 and Tyr 68.

A hydrogen bonding pattern commonly seen in the peptide of Grb2-SH2 domain/phosphopeptide complexes is from the backbone carbonyl of pTyr to the backbone amide of the +3 residue (in this case Gln 1142) (Nioche et al., 2002). Involvement of the backbone amide proton of +1 Val 1140 in a hydrogen bond to the backbone carbonyl oxygen of +3 Gln 1142 is seen in most of the calculated structures (Figure 8C); making Gln 1142 a participant in the bound turn structure of pY1139. The existence of interactions between backbone atoms of Val 1140 and Gln 1142 does not explain potential effects on specificity via this residue. Presumably any residue at this +3 position, barring proline, could interact in such a manner to stabilize a turn conformation.

For most SH2 domains, the introduction of a leucine at the βD6 position, such as in hGrb7, removes an important amino-aromatic interaction to the RTK phosphotyrosine aromatic ring at this highly conserved residue (Waksman et al., 1993; Pascal et al., 1994; Ogura et al., 1999). Among all of the known proteins containing SH2 domains, only the Grb7-SH2 domain and the C-terminal SH2 domain of the p85α subunit of phosphatidylinositol 3-kinase do not have an Arg, Lys or Gln at this position. The C-terminal SH2 domain of the p85α subunit of phosphatidylinositol 3-kinase appears to make up for the lost interaction by having a lysine in the BC3 loop position in a geometry which could regain the amino-aromatic interaction (Breeze et al., 1996). Grb7 has an asparagine at this BC3 position (Asn 51). While asparagine does contain an amide in its side chain, the hydrogen bonding patterns observed in the structures presented imply that Asn 51 is indirectly involved in a stabilizing interaction with the phosphate group of pTyr 1139, and not in an amino-aromatic interaction. Instead, the leucine in the βD6 position (Leu 69) provides the main stabilizing force for the pTyr 1139 aromatic ring via hydrophobic packing with its methyl groups (Figure 8B). The βD6 residue *sidechain* is not known to interact with the +1 to the +3 residues in SH2 domain-peptide binding (Waksman et al., 1993; Pascal et al., 1994; Ogura et al., 1999), so the change in specificity in the βD6 position of Grb7 and Grb14 is difficult to explain. The binding to the pYVNQ peptide seen in the βD6 Grb14-SH2 mutant may be a result of a different binding geometry to the phosphotyrosine aromatic ring owing to hydrophobic-hydrophobic interactions versus that of the amino-aromatic interaction normally seen in SH2 domain-phosphotyrosine binding studies (Waksman et al., 1993, Pascal et al., 1994, Ogura et al., 1999). It is also possible that introduction of a glutamine in the βD6 position, as in hGrb14, may change the electrostatic potential in this region and the ability of hGrb7 to bind pYXN(Q/R) peptides.

Conclusions

The solution structure of the human Grb7-SH2 domain in complex with a ten amino acid phosphorylated tyrosine peptide representative of the erbB2 Grb7 binding site (pY1139) has been elucidated. The bound conformation of the pY1139 peptide on hGrb7-SH2 domain is in a tight β-turn, as a result of the four residue insertion present in the region between the βE strand and the EF loop of the hGrb7-SH2 domain. Stabilizing contacts between the pY1139 peptide and the

hGrb7-SH2 domain include pTyr 1139 phosphate/Arg 46 and pTyr 1139 phosphate/Ser 48 ionic interactions within the standard SH2 domain phosphotyrosine binding pocket, as well as hydrophobic interactions between the SH2 domain βD5 residue/pY1139 +1 valine methyl groups and the SH2 domain βD6 residue/pY1139 pTyr aromatic ring. Additional stabilizing contacts are seen between the SH2 domain βE residue Ser 82 sidechain and the pY1139 +2 asparagine sidechain, mimicking a phosphotyrosine peptide – protein interaction observed in published Grb2-SH2 domain/pTyr peptide complex structures. The importance of the βD5, βD6 hGrb7-SH2 domain residues in binding pY1139 is demonstrated by the close contacts observed. However, differences in specificity between hGrb7 and hGrb14 arising from mutation of these two residues is not fully explained, particularly with relation to potential interactions between the SH2 domain and the +3 glutamine residue subsequent to the phosphotyrosine. Further structural characterization of βD5/βD6 hGrb7-SH2 and hGrb14-SH2 domain mutants is underway to clarify the role of the phosphopeptide +3 residue position in Grb7 protein binding specificity.

The ^{1}H, ^{15}N and ^{13}C assignments and the atom coordinates have been deposited in the BioMagResBank (accession code BMRB-5288) and in the Protein Data Bank (PDB code 1MW4), respectively.

Acknowledgements

The authors wish to thank Tracy Handel and Peter Domaille for many helpful discussions ranging from ANSIG trivia to current ski conditions.

References

Azara, v2.0, copyright (C) 1993–1996 Wayne Boucher and Department of Biochemistry, University of Cambridge, Cambridge.

Booker, G.W., Breeze, A.L., Downing, A.K., Panayotou, G., Gout, I., Waterfield, M.D. and Campbell, I.D. (1992) *Nature*, **358**, 684–687.

Breeze, A.L., Kara, B.V., Barratt, D.G., Anderson, M., Smith, J.C., Luke, R.W., Best, J. R. and Cartlidge, S.A. (1996) *EMBO J.*, **15**, 3579–3589.

Brescia, P.J., Ivancic, M. and Lyons, B.A. (2002) *J. Biomol. NMR*, **23**, 77–78.

Brunger, A.T., Adams, P.D., Clore, G.M., DeLano, W.L., Gros, P., Grosse-Kunstleve, R.W., Jiang, J.S., Kuszewski, J., Nilges, M., Pannu, N.S., Read, R.J., Rice, L.M., Simonson, T. and Warren, G.L. (1998) *Acta Cryst.*, **D54**, 905–921.

Choi, G., Ha, N.C. Kim, M.S., Hong, B.H., Oh, B.H. and Choi, K.Y. (2001) *Biochemistry*, **40**, 6828–6835.

Clore, G.M., Kay, L.E., Bax, A. and Gronenborn, A.M. (1991) *Biochemistry*, **30**, 12–18.

Daly, R. J., Sanderson, G. M., Janes, P. W. and Sutherland, R. L. (1996) *J. Biol. Chem.*, **271**, 12502–12510.

Eck, M.J., Shoelson, S.E. and Harrison, S.C. (1993) *Nature*, **362**, 87–91.

Fiddes, R.J., Campbell, D.H,, Janes, P.W., Sivertsen, S.P., Sasaki, H., Wallasch, C. and Daly, R.J. (1998) *J. Biol. Chem.*, **273**, 7717–7724.

Forman-Kay, J.D., Gronenborn, A.M., Kay, L.E., Wingfield, P.T. and Clore, G.M. (1990) *Biochemistry*, **29**, 1566–1572.

Guan, K.L. and Dixon, J.E., (1991) *Anal. Biochem.*, **192**, 262–267.

Guex, N. and Peitsch, M.C. (1997) *Electrophoresis*, **18**, 2714–2723.

He, W., Rose, D.W., Olefsky, J.M. and Gustafson, T.A. (1998) *J. Biol. Chem.*, **273**, 6860–6867.

Helgstrand, M., Kraulis, P., Allard, P. and Hard, T. (2000) *J. Biomol. NMR*, **18**, 329–336.

Janes, P.J., Lackmann, M., Church, W.B., Sanderson, G.M., Sutherland, R.L. and Daly, R.J. (1997) *J. Biol. Chem.*, **272**, 8490–8497.

Kay, L.E. (1995) *Prog. Biophys. Mol. Biol.*, **63**, 277–299.

Kay, L.E. and Bax, A. (1990) *J. Magn. Reson.*, **86**, 110–126.

Kay L.E., Keifer, P. and Saarinen, T. (1992) *J. Am. Chem. Soc.*, **114**, 10663–10665

Kraulis, P.J. (1989) *J. Magn. Reson.*, **84**, 627–633.

Kraulis, P.J, Domaille, P.J, Campbell-Burk, S.L., van Aken, T. and Laue, E.D. (1994) *Biochemistry*, **33**, 3515–3531.

Kuszewski, J., Qin, J., Gronenborn, A.M. and Clore, G.M. (1995) *J. Magn. Reson.*, **B106**, 92–96.

Laskowski, R.A., Macarthur, M.W., Moss, D.S. and Thornton, J.M. (1993) *J. Appl. Crystallogr.*, **26**, 283–291.

Lovell, S.C., Word, J.M., Richardson, J.S. and Richardson, D.C. (2000) *Proteins*, **40**, 389–408.

Margolis, B. (1994) *Prog. Biophys. Mol. Biol.*, **62**, 223–244.

Margolis, B., Silvennoinen, O., Comoglio, F., Roonprapunt, C., Skolnik, E., Ullrich, A. and Schlessinger, J. (1992) *Proc. Natl. Acad. Sci. USA*, **89**, 8894–8898.

Marion, D., Driscoll, P.C., Kay, L.E., Wingfield, P.T., Bax, A., Gronenborn, A.M. and Clore, G.M. (1989) *Biochemistry*, **28**, 6150–6156.

McNemar, C., Snow, M.E., Windsor, W.T., Prongay, A., Mui, P., Zhang, R., Durkin, J., Le, H.V. and Weber, P.C. (1997) *Biochemistry*, **36**, 10006–10014.

Morrione, A., Plant, P., Valentinis, B., Staub, O., Kumar, S., Rotin, D. and Baserga, R. (1999) *J. Biol. Chem.*, **274**, 24094–24099.

Nantel, A., Mohammad-Ali, K., Sherk, J., Posner, B.I. and Thomas, D.Y. (1998) *J. Biol. Chem.*, **273**, 10475–10484.

Nioche, P., Liu, W.Q., Broutin, I., Charbonnier, F., Latreille, M.T., Vidal, M., Roques, B., Garbay, C. and Ducruix, A. (2002) *J. Mol. Biol.*, **315**, 1167–1177.

Ogura, K., Tsuchiya, S., Terasawa, H., Yuzawa, S., Hatanaka, H., Mandiyan, V., Schlessinger, J. and Inagaki, F. (1999) *J. Mol. Biol.*, **289**, 439–445.

Otting, G. and Wüthrich, K. (1990) *Quart. Rev. Biophys.*, **23**, 39–96.

Pandey, A., Duan, H., Di Fiore, P.P. and Dixit, V.M. (1995) *J. Biol. Chem.*, **270**, 21461–21463.

Pascal, S.M., Singer, A.U., Gish, G., Yamazaki, T., Shoelson, S.E., Pawson, T., Kay, L.E. and Forman-Kay, J. (1994) *Cell*, **77**, 461–472.

Rahuel, J., Garcia-Echeverria, C., Furet, P., Strauss, A., Caravatti, G., Fretz, H., Schoepfer, J. and Gay, B. (1998) *J. Mol. Biol.*, **279**, 1013–1022.

Reilly, J.F., Mickey, G. and Maher, P.A. (2000) *J. Biol. Chem.* **275**, 7771–7778.

Stein, D., Wu, J., Fuqua, S.A., Roonprapunt, C., Yajnik, V., D'Eustachio, P., Moskow, J.J., Buchberg, A.M., Osborne, C.K. and Margolis, B. (1994) *EMBO J.*, **13**, 1331–1340.

Stein, E.G., Ghirlando, R. and Hubbard, S.R. (2003) *J. Biol. Chem.*, in press.

Thommes, K., Lennartsson, J., Carlberg, M. and Ronnstrand, L. (1999) *Biochem. J.*, **341**, 211–216.

Thornton, K.H., Mueller, W.T., McConnell, P., Zhu, G., Saltiel, A.R. and Thanabal, V. (1996) *Biochemistry*, **35**, 11852–11864.

Waksman, G., Shoelson, S.E., Pant, N, Cowburn, D. and Kuriyan, J. (1993) *Cell*, **72**, 779–790.

Wang, J., Dai, H., Yousaf, N., Moussaif, M., Deng, Y., Boufelliga, A., Swamy, O.R., Leone, M.E. and Riedel, H. (1999) *Mol. Cell. Biol.*, **19**, 6217–6228.

Wang, Y.S., Frederick, A.F., Senior, M.M., Lyons, B.A., Black, S., Kirschmeier, P., Perkins, L.M. and Wilson, O. (1996) *J. Biomol. NMR*, **7**, 89–98.

Wishart, D.S., Bigam, C.G., Yao, J., Abildgaard, F., Dyson, H.J., Oldfield, E., Markley, J.L. and Sykes, B.D. (1995) *J. Biomol. NMR*, **6**, 135–140.

Wojcik, J., Girault, J.A., Labesse, G., Chomilier, J., Mornon, J.P. and Callebaut, I. (1999) *Biochem. Biophys. Res. Commun.*, **259**, 113–120.

Zhang, O., Kay, L.E., Olivier, J.P. and Forman-Kay, J.D. (1994) *J. Biomol. NMR*, **4**, 845–858.